Supporting Information:

Atomic-Scale Structural Mechanisms Governing Dopant-Induced Stabilization and Photoluminescence Enhancement in $CsPbI_3$ Quantum Dots

Yue Yin,[a] Yanan Qi,[a] Le Fang,[b] Andrei Sapelkin,[c] Martin T Dove, [d, e,] [c]Haijun Huang,[a] Jianrong Zeng,[f, g] and Lei Tan * [a]

[a] Department of Physics, School of Physics and Mechanics, Wuhan University of Technology, Wuhan, Hubei 430070, China

[b] School of Life and Health Sciences, Hubei University of Technology, Wuhan 430068, China

[c] School of Physical and Chemical Sciences, Queen Mary University of London, Mile End Road, London, E1 4NS, UK

[d] School of Mechanical Engineering, Guizhou University of Engineering Science, Bijie, Guizhou, 55170, China

[e] Institute of Atomic and Molecular Physics, Sichuan University, Chengdu, 610065, P. R. China

[f] Shanghai Synchrotron Radiation Facility, Shanghai Advanced Research Institute, Chinese Academy of Sciences, 201204 Shanghai, China.

[g] Shanghai Institute of Applied Physics, Chinese Academy of Sciences, 201800 Shanghai, China.

E-mail: lei.tan@whut.edu.cn

Contents

Section S1: Synthesis and Characterization of quantum dots

Chemicals. Cesium carbonate (Cs_2CO_3, Adamas, 99.9%), lead iodide (PbI_2, J&K, 99.999%), 1-octadecene(ODE, Adamas, 90%), zinc iodide (ZnI_2, Adamas, 99.99%), hexane (97%, Adamas), oleylamine (OAm, Adamas, 90%), oleic acid (OA, Adamas, 90%), methyl acetate (MeOAc, Adamas, 99%). All chemicals were used as received without further purification.

Preparation of Precursors. Cs_2CO_3 (400 mg), 10 mL ODE and 1.6 mL OA were mixed in a 100 mL three-necked flask. The mixture was dried for 30 minutes under vacuum at 120 ℃. The vacuum and N_2 were alternated three times for another 30 minutes. Then, the mixture was heated to 150 ℃ under N_2 until all Cs_2CO_3 dissolved. Since Cs-oleate precipitates out of ODE at room-temperature, it has to be preheated to 70 ℃ before injection.

Synthesis of $CsPbI_3$ QDs. $CsPbI_3$ QDs were synthesized by a hot injection method[1]. PbI_2 (0.173 g) and 10 ml ODE were mixed in a 100 ml Schlenk flask and dried for 1 h under vacuum at 120 ℃ . OA (1 mL) and OAm (1 mL) were injected at 120 ℃ under N_2. The flask was put under vacuum again until the PbI_2 completely dissolved. The temperature was increased to 170 ℃ and Cs-oleate solution (1.6 mL) was swiftly injected. Then, the flask was quenched with an ice-water bath.

Synthesis of $CsPb_{1-x}Zn_xI_3$ QDs. PbI_2 (0.173 g), ZnI_2 (0.06 g, 0.081 g, 0.09 g, 0.12 g, 0.15 g) and 10 ml ODE were mixed in a 100 ml Schlenk flask and dried for 1 h under vacuum at 120 ℃. The following steps were the same with the synthesis of the $CsPbI_3$ QDs. OA (1 mL) and OAm (1 mL) were injected at 120 ℃ under N_2. The flask was put under vacuum again until the PbI_2 and ZnI_2 completely dissolved. The temperature was increased to 170 ℃ and Cs-oleate solution (1.6 mL) was swiftly injected. After 5 s of the reaction time, the flask was quenched with an ice-water bath.

Purification. The resulting quantum dots were purified twice with methyl acetate to remove unreacted precursors[2]. Methyl acetate (20 mL) was added to the crude solution, and the mixture was centrifuged for 5 min at 8000 rpm. After that, the supernatant was discarded. The precipitate was dispersed in 6 ml hexane and 6 ml MeOAc, the mixture were centrifuged for 5 min at 8000 rpm. The supernatant was then discarded, and the precipitate was collected. All the following process were peformed in the glovebox.

Characterization. X-ray diffraction (XRD) patterns were acquired using a Empyrean X-ray diffractometer with a Cu Kα radiation sourcea at 40 kV and 40 mA. The samples were scanned over a 2θ range of 10-80° with a slow scan rate for 15 minutes. The photoluminescence (PL) spectra were recorded at an excitation wavelength of 400 nm using a FluoroMax-4 fluorescence spectrophotometer. The absolute PL

quantum yield (PLQY) of the samples was measured on a fluorescence spectrometer (FLS1000, Edinburgh Instruments) equipped with an integrating sphere, with excitation provided by a 400 nm xenon lamp. Energy-dispersive X-ray spectroscopy (EDS) was performed on a Talos F200S transmission electron microscope operated at an accelerating voltage of 200 kV. Pair distribution function (PDF) were also collected at the BL13SSW beamline at the Shanghai Synchrotron Radiation Facility (SSRF) using a 50 keV X-ray beam. An additional dataset for the Zn/Pb=0.5 sample measured at BL12SSW using a wavelength of 0.1275 Å. Samples were loaded into specialized glass tubes with a diameter of 1.5 mm. The extended X-ray absorption fine structure spectra (EXAFS) were also collected at the BL13SSW beamline at the Shanghai Synchrotron Radiation Facility (SSRF). The energy was calibrated with reference to the pure Pb foil absorption edge. Measurements were scanned with constant speed using Si (111) crystal.

Section S2. Photoluminescence (PL)

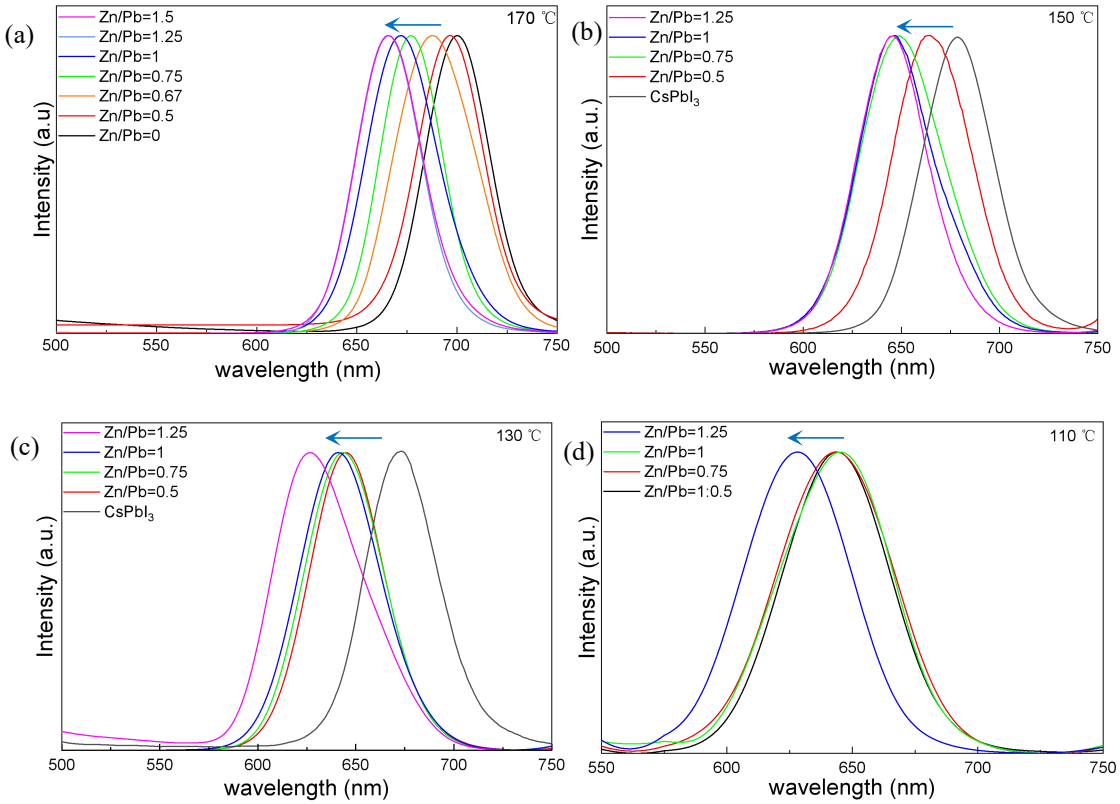

Figure S1. Normalized PL spectrum of $CsPbI_3$ and $CsPb_{1-x}Zn_xI_3$ QDs. (a) 170 ℃, (b) 150 ℃, (c) 130 ℃, (d) 110 ℃. PL spectrum have a blue shift trend with the increase in Zn ratio. Meanwhile, PL spectrum also have a blue shift trend with the decrease temperature.

Section S3. X-ray diffraction (XRD)

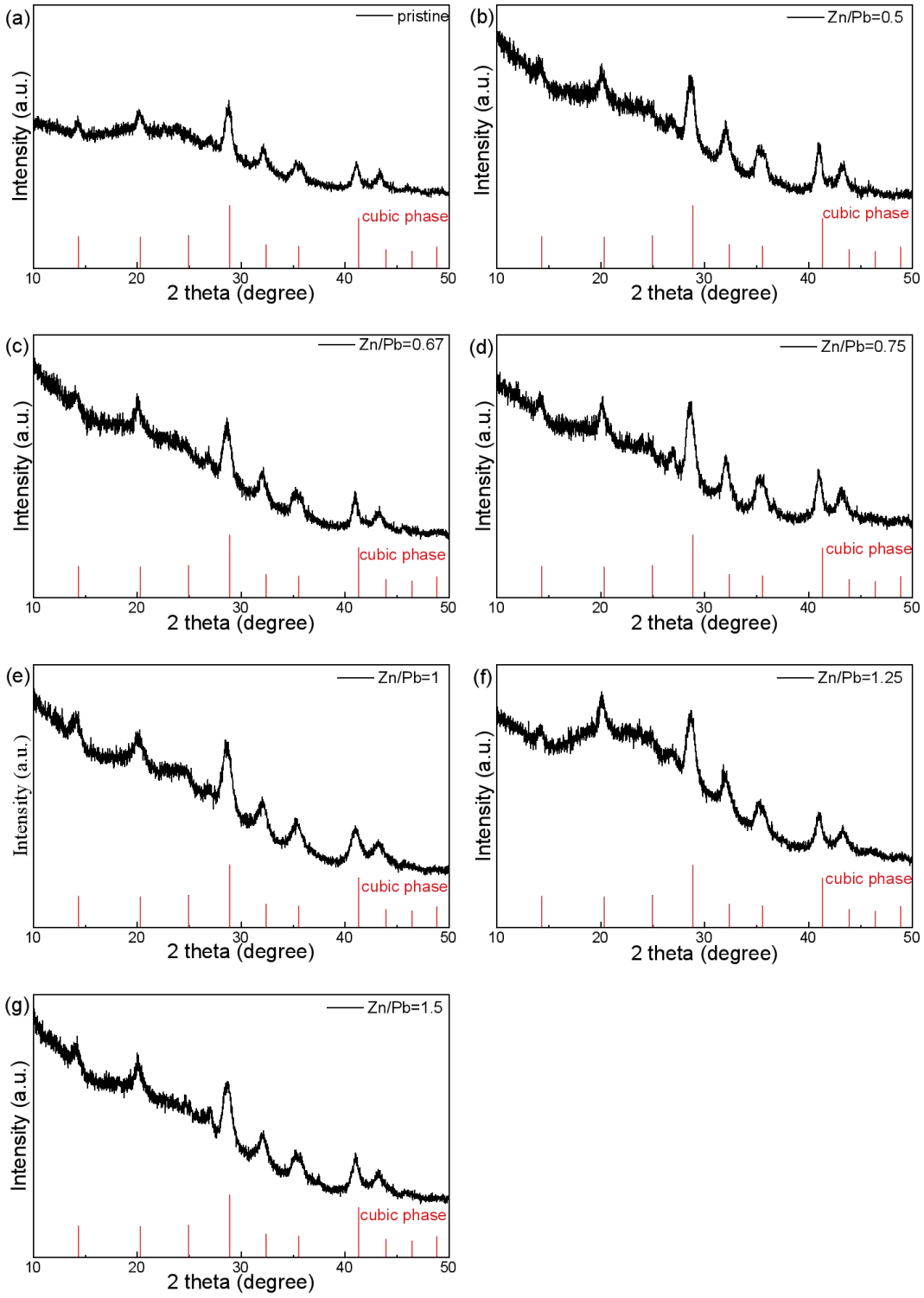

Figure S2. XRD patterns for pristine $CsPbI_3$ and different $CsPb_{1-x}Zn_xI_3$ QDs with Zn/Pb moler ratios of (a) 0, (b) 0.5, (c) 0.67, (d) 0.75, (e) 1, (f) 1.25, (g) 1.5. All the samples were cubic phase, the lattice structure of the QDs remained unchanged.

Section S4. Energy Dispersive X-ray Spectroscopy (EDS)

The EDS of differernt samples were was performed on a Talos F200S transmission electron microscope using the same conditions, and all the samples were dissolved in hexane and ultrasonicated prior to testing. EDS can measure the concentrations of various constituent elements in the differernt QDs. The detailed results are as follows.

Table S1. Mass ratios of constituent elements inside the $CsPb_{1-x}Zn_xI_3$ QDs

Sample	Zn/Pb	Cs	Pb	I	Experimental Zn	Theoretical Zn
$CsPbI_3$	0	0.998	1	2.769	0	0
$CsPb_{0.67}Zn_{0.33}I_3$	0.5	0.978	1	3.263	0.169	0.158
$CsPb_{0.6}Zn_{0.4}I_3$	0.67	0.914	1	3.348	0.224	0.212
$CsPb_{0.57}Zn_{0.43}I_3$	0.75	0.969	1	3.560	0.247	0.237
$CsPb_{0.5}Zn_{0.5}I_3$	1	1.053	1	3.722	0.274	0.316
$CsPb_{0.44}Zn_{0.56}I_3$	1.25	0.997	1	3.363	0.351	0.395
$CsPb_{0.4}Zn_{0.6}I_3$	1.5	0.910	1	3.654	0.500	0.474

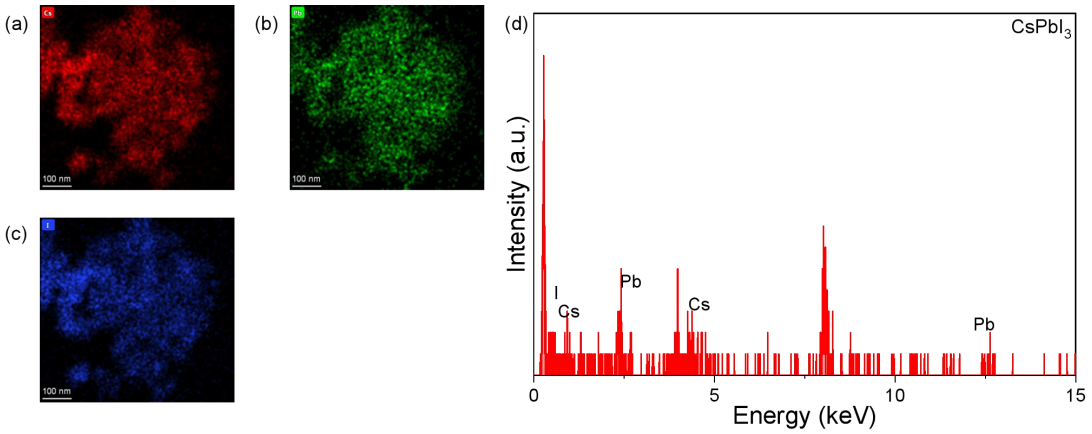

Figure S3. Elemental mapping images of (a) Cs, (b) Pb, (c) I for $CsPbI_3$ QDs. (d) EDS spectrum for $CsPbI_3$ QDs.

Section S5. Photoluminescence Quantum Yield (PLQY)

The PLQY of the different samples was measured using an integrating sphere attached to a spectrofluorometer (FLS1000, Edinburgh Instruments) with excitation at 400 nm. All samples were dispersed in hexane prior to measurement.

Table S2. The PLQY of pristine $CsPbI_3$ and $CsPb_{1-x}Zn_xI_3$ QDs.

Temperature (℃)	Sample	ratio	PLQY (%)
170	$CsPbI_3$	Zn/Pb=0	24
170	$CsPb_{0.67}Zn_{0.33}I_3$	Zn/Pb=0.5	49
170	$CsPb_{0.6}Zn_{0.4}I_3$	Zn/Pb=0.67	71
170	$CsPb_{0.57}Zn_{0.43}I_3$	Zn/Pb=0.75	76
170	$CsPb_{0.5}Zn_{0.5}I_3$	Zn/Pb=1	88
170	$CsPb_{0.44}Zn_{0.56}I_3$	Zn/Pb=1.25	97
170	$CsPb_{0.4}Zn_{0.6}I_3$	Zn/Pb=1.5	82

Section S6. Photoluminescence lifetime

Photoluminescence lifetime acquired using an integrating sphere incorporated into a spectrofluorometer (FLS1000, Edinburgh Instruments), an excitation wavelength of 400 nm and the same excitation power were employed. All the samples were dispersed in hexane. Time-resolved PL decay curves were fitted to a bi-exponential decay curves, and the average lifetimes were calculated using S2[3].

bi-exponential decay: $I = A_1 \exp(-t/\tau_1) + A_2 \exp(-t/\tau_2)$ (1)

PL average lifetime: $\tau_{avg} = \frac{A_1\tau_1^{\ 2} + A_2\tau_2^{\ 2}}{A_1\tau_1 + A_2\tau_2}$ (2)

radiative lifetime: $\tau_r = \frac{\tau_{avg}}{QY}$ (3)

apparent nonradiative lifetime: $\tau_{nr} = \frac{\tau_{avg}}{1-QY}$ (4)

radiative decay rate: $k_r = \frac{1}{\tau_r}$ (5)

apparent nonradiative decay rate: $k_{nr} = \frac{1}{\tau_{nr}}$ (6)

Table S3. The average lifetimes (τ_{avg}), radiative lifetime (τ_r) and apparent nonradiative lifetime (τ_{nr}), radiative decay rate (k_r) and apparent nonradiative decay rate (k_{nr}) of $CsPbI_3$ and $CsPb_{1-x}Zn_xI_3$ QDs.

Sample	τ_1 (ns)	A_1 (%)	τ_2 (ns)	A_2 (%)	τ_{avg} (ns)	τ_r (ns)	τ_{nr} (ns)	k_r (ns^{-1})	k_{nr} (ns^{-1})
$CsPbI_3$	7.65	0.55	41.01	0.38	33.9	141	44	0.007	0.02
$CsPb_{0.67}Zn_{0.33}I_3$	3.53	0.61	29.88	0.34	25.3	51.6	49	0.019	0.02
$CsPb_{0.6}Zn_{0.4}I_3$	11.92	0.44	65.88	0.42	57.3	80.7	197	0.012	0.005
$CsPb_{0.57}Zn_{0.43}I_3$	8.16	0.42	20.52	0.59	33	43.4	137	0.023	0.007
$CsPb_{0.5}Zn_{0.5}I_3$	5.98	0.35	28.02	0.60	26	29.5	216	0.034	0.005
$CsPb_{0.44}Zn_{0.56}I_3$	7.60	0.32	25.92	0.66	24	24.7	800	0.040	0.001
$CsPb_{0.4}Zn_{0.6}I_3$	6.01	0.36	30.76	0.60	28.1	34.3	156	0.029	0.006

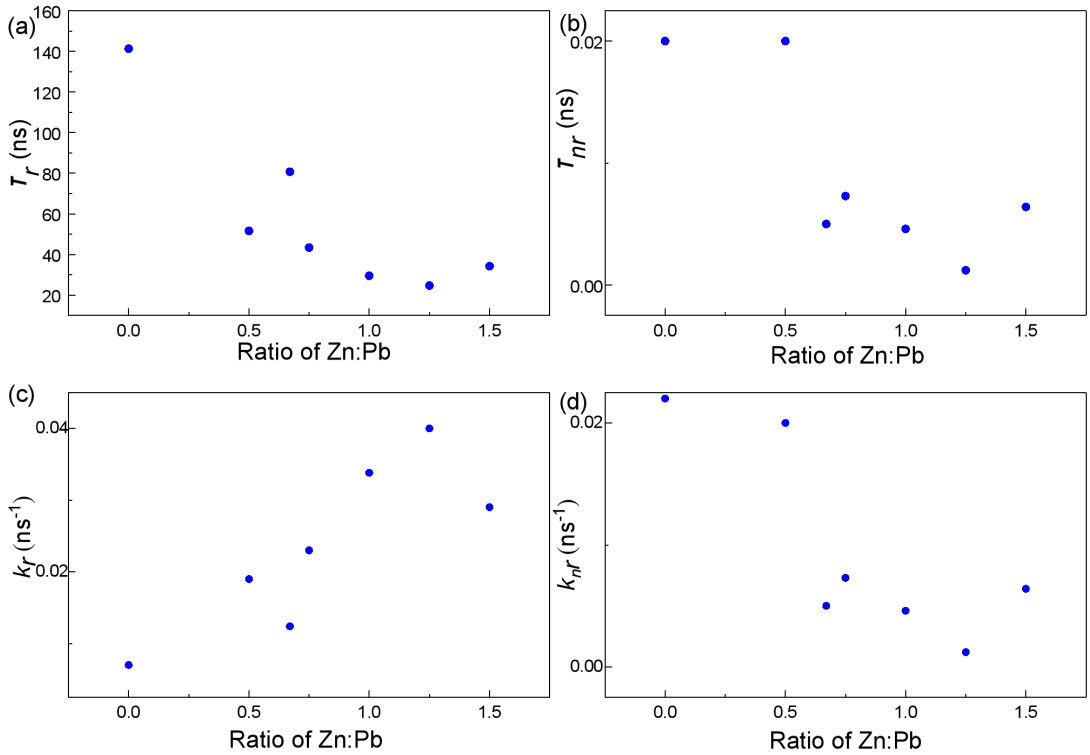

Figure S4. Radiative lifetime (a) and apparent nonradiative lifetime (b) of $CsPbI_3$ and $CsPb_{1-x}Zn_xI_3$ QDs with different Zn/Pb moler ratios. The radiative decay rate (c) and apparent nonradiative decay rate (d) of $CsPbI_3$ and $CsPb_{1-x}Zn_xI_3$ QDs with different ZnI_2-to-PbI_2 ratios.

Section S7. X-ray total scattering

X-ray total scattering combined with pair distribution function (PDF) analysis provides direct access to local and intermediate-range atomic structure beyond the information obtainable from conventional Bragg diffraction. By simultaneously accounting for both Bragg and diffuse scattering, PDF analysis is particularly well suited for disordered and nanocrystalline systems such as perovskite quantum dots.

The experimentally measured quantity is the total scattering structure function, S(Q), where $Q=4\pi\sin\theta/\lambda$ is the magnitude of the scattering vector. The reduced structure function is defined as $F(Q)=Q[S(Q)-1]$, and the real-space PDF, D(r), is obtained by Fourier transformation of F(Q).

$$D(r) = \frac{2}{\pi}\int_{Q_{\min}}^{Q_{\max}} F(Q)\sin(Qr)\,dQ \tag{7}$$

The PDF represents the probability of finding pairs of atoms separated by a distance r, with distinct peaks corresponding to characteristic interatomic separations.The maximum momentum transfer Q_{max} determines the real-space resolution of the PDF, with higher Q_{max} enabling more accurate characterization of local bonding and structural disorder. As a result, PDF analysis allows quantitative determination of bond lengths, coordination environments, and local structure distortions that are not captured by average crystallographic models.

In this work X-ray total scattering data were collected at the BL13SSW beamline at the Shanghai Synchrotron Radiation Facility (SSRF) using a 50 keV X-ray beam, using an incident wavelength of 0.248 Å. An additional dataset for the Zn/Pb=0.5 sample measured at BL12SSW using a wavelength of 0.1275 Å. CeO_2 was used as the standard sample for the instrument parameter calibration. The QDs were loaded into specialized glass tubes with a diameter of 1.5 mm, and were tested for 400 s. In addition to the sample measurements, separate measurements of the empty glass tubes were performed for data correction purposes. Then, the fitting of the theoretical model to the experimental X-ray total scattering data was performed using PDFgui[4] software to obtain the local structure of different QDs. The X-ray total scattering data collected at beamline BL13SSW were Fourier-transformed using Q_{min}=1.5 $Å^{-1}$ and Q_{max}=16 $Å^{-1}$ to obtain the PDF. For the dataset acquired at beamline BL12SSW, which utilized a higher incident X-ray energy, a Q_{max} of 21 $Å^{-1}$ was applied during data processing.

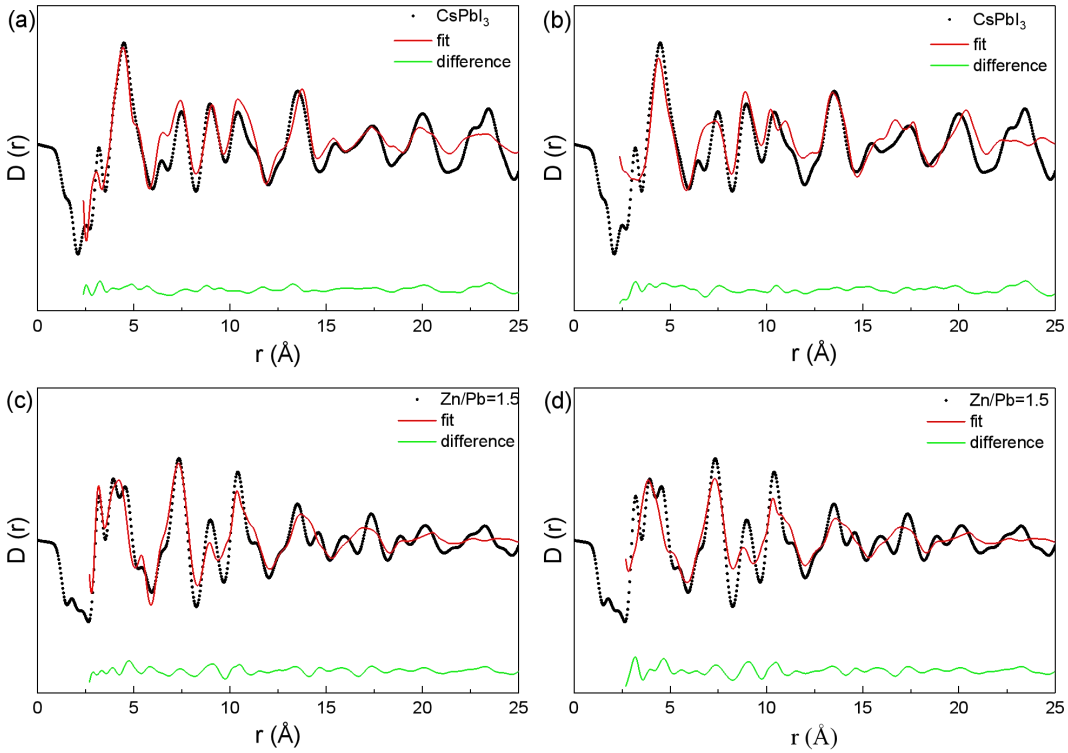

Figure S5. PDFs extracted from synchrotron X-ray total scattering data collected on $CsPbI_3$ and $CsPb_{0.4}Zn_{0.6}I_3$ QDs (Zn/Pb=1.5) with different structural models, (a, c) mixture of alpha and delta phase, (b, d) delta phase. The red line indicates different models fit to the PDFs. The lines at the bottom of the panels indicate the difference between the PDF and the fits.

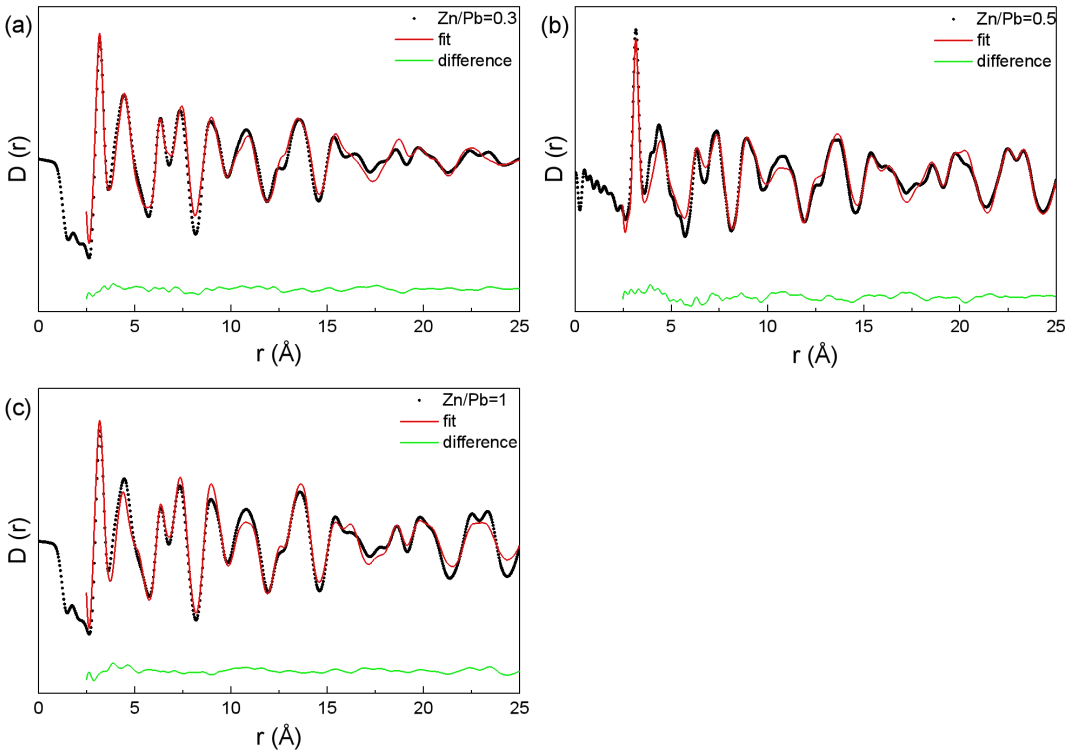

Figure S6. PDFs extracted from synchrotron X-ray total scattering data collected on different $CsPb_{1-x}Zn_xI_3$ QDs with Zn/Pb moler ratios of (a) 0.3, (b) 0.5 and (c) 1. The red line indicates gama phase model fit to the PDFs. The lines at the bottom of the panels indicate the difference between the PDF and the fit.

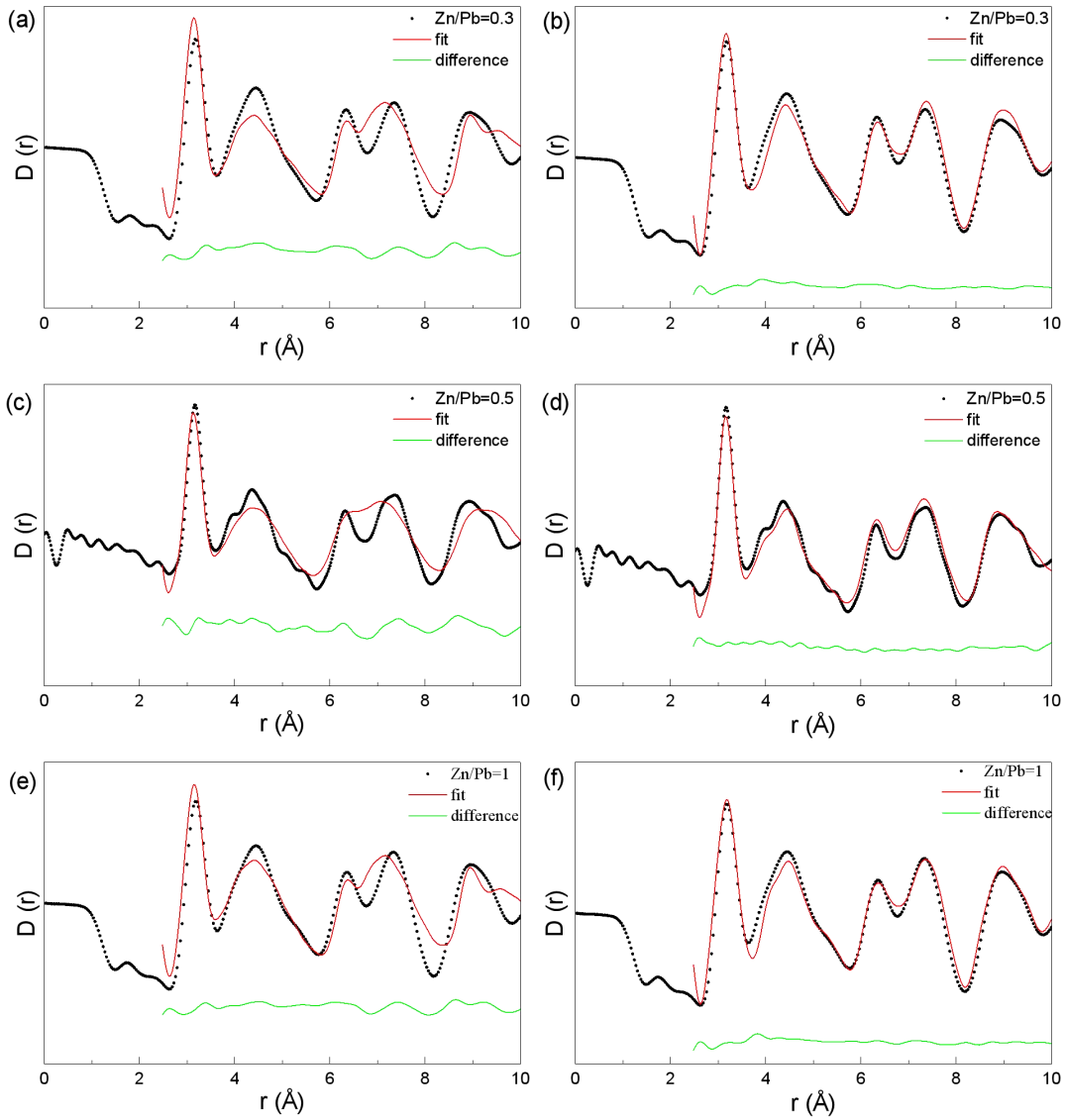

Figure S7. PDFs extracted from synchrotron X-ray total scattering data collected on $CsPb_{1-x}Zn_xI_3$ QDs with ZnI_2-to-PbI_2 ratios with different structural models, (a, c, e) alpha phase, (b, d, f) gama phase. The red line indicates different models fit to the PDFs. The lines at the bottom of the panels indicate the difference between the PDF and the fits.

Section S8. X-ray absoprtion experiment

EXAFS measured the samples' Pb L_3-edge (13035 eV) and the spectra were obtained under fluorescence mode.The energy was calibrated with reference to the pure Pb foil absorption edge. Measurements were done in quick scanning mode, where the undulator gap and taper were fixed for each edge while the Bragg angle of the double crystal monochromator. Measurements were scanned with constant speed using Si (111) crystal. Data were processed using Athena software.The normalization process was carried out using the Athena software, which employs an automated algorithm to consistently determine the pre-edge and post-edge regions for optimal background removal[5]. The energy calibration was performed using a standard Pb foil reference prior to normalization to ensure the accuracy of the processed EXAFS spectra. Then, the fitting of the theoretical model to the experimental EXAFS data was performed using Artemis software with FEFF6 to obtain the local structure around Pb. The fitting was conducted for the Pb-I coordination shell within the range of 1.8-3.2 Å using Fourier transform (FT) analysis in R space. The fitting employed a CIF model with the cubic space group of $CsPbI_3$ to obtain information such as the coordination number, bond length (R), and Debye-Waller factor (σ^2). Cubic-phase $CsPbI_3$ was used as a reference standard, and the coordination number was fixed at 6 to determine the amplitude reduction factor (S_0^2), which was found to be 0.56. This value was subsequently fixed for EXAFS fitting of all quantum dot samples. It is worth noted that all fits yielded R-factors below 0.02, confirming the reliability and accuracy of the extracted structural parameters. In addition, we measured the Zn K-edge (9659 eV) data of Zn-doped quantum dots with different doping ratios. The spectra qualitatively confirm successful Zn incorporation in the samples. However, due to the relatively weak Zn K-edge signal and limited signal-to-noise ratio, the data quality is insufficient for reliable quantitative EXAFS fitting analysis.

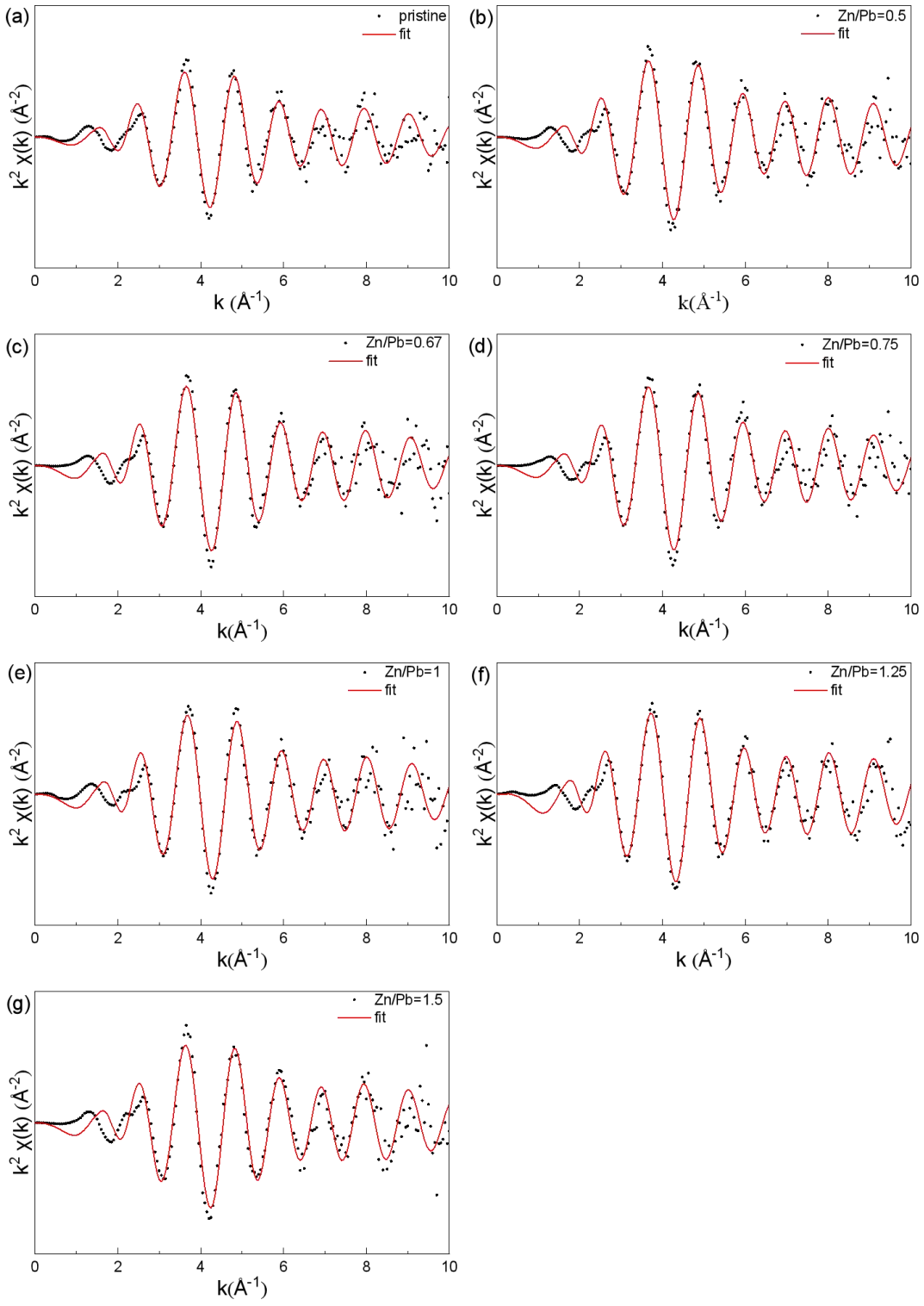

Figure S8. k^2-weighted Pb L_3-edge EXAFS data and fits for $CsPbI_3$ and different $CsPb_{1-x}Zn_xI_3$ QDs with Zn/Pb moler ratios of (a) 0, (b) 0.5, (c) 0.67, (d) 0.75, (e) 1, (f) 1.25, (g) 1.5. The red line indicates cubic model fit to the EXAFS data.

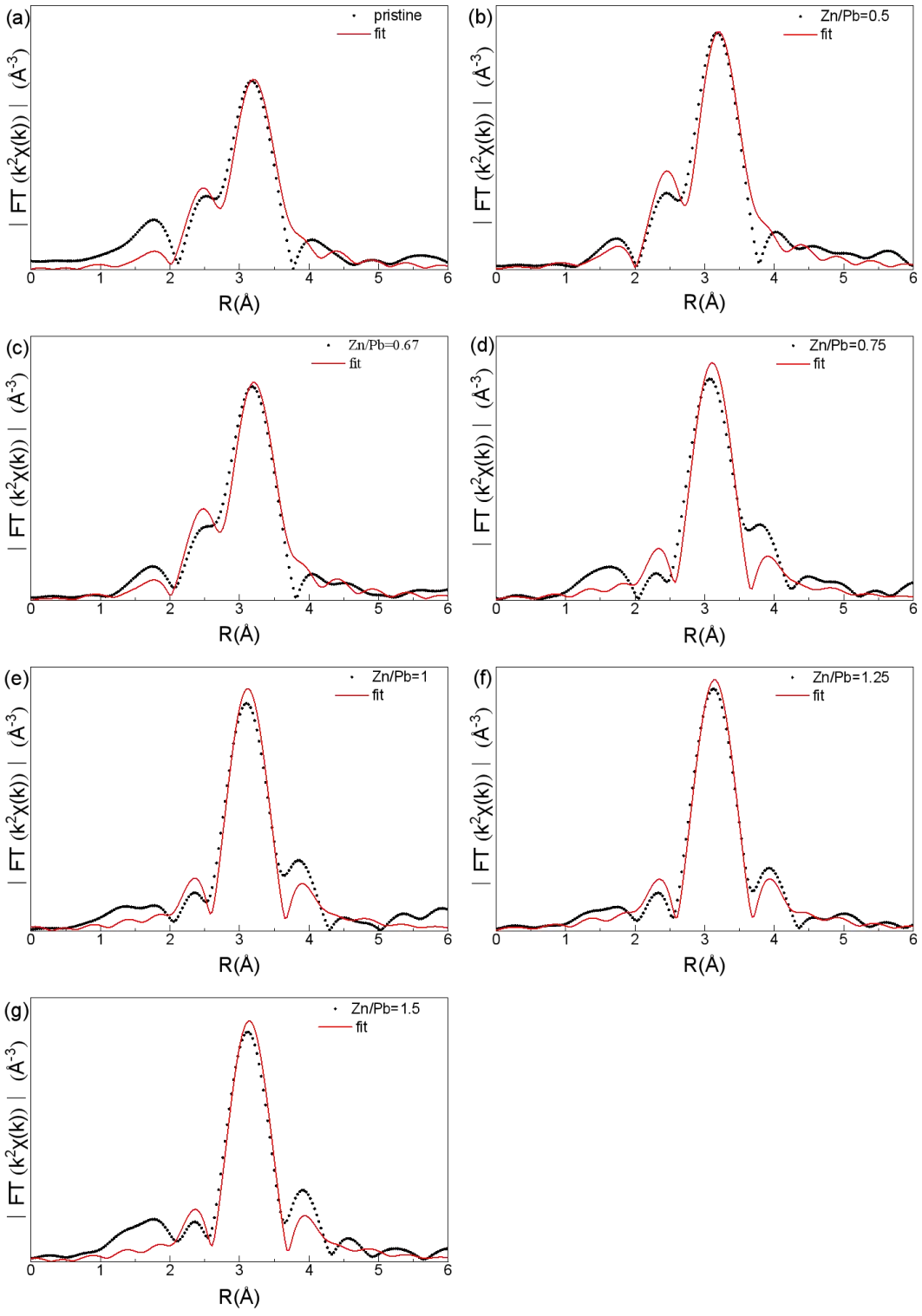

Figure S9. Corresponding fourier transforms and fits for $CsPbI_3$ and different $CsPb_{1-x}Zn_xI_3$ QDs with Zn/Pb moler ratios of (a) 0, (b) 0.5, (c) 0.67, (d) 0.75, (e) 1, (f) 1.25, (g) 1.5. The red line indicates cubic model fit to the fourier transforms.

Wavelet transform was applied to the k^2-weighted EXAFS signal using hama Fortran[6]. The fitting is performed using the Morlet function with κ and σ set to 8 and 1, respectively. The R ranges were set to be 0-6 Å.

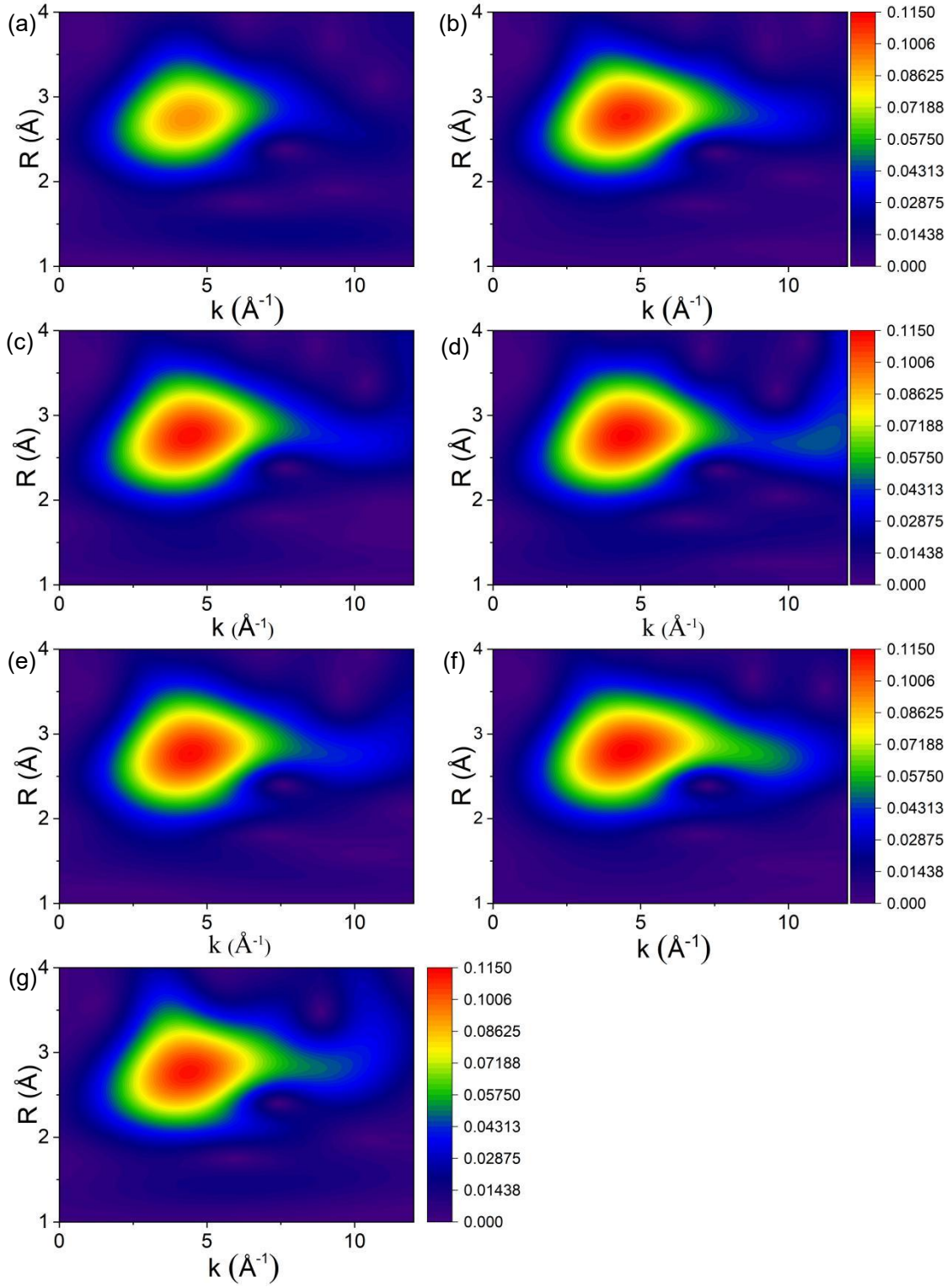

Figure S10. Wavelet transform of k^2-weighted Pb L_3-edge EXAFS data for and fits for $CsPbI_3$ and different $CsPb_{1-x}Zn_xI_3$ QDs with Zn/Pb moler ratios of (a) 0, (b) 0.5, (c) 0.67, (d) 0.75, (e) 1, (f) 1.25, (g) 1.5. The color scale represents intensity.

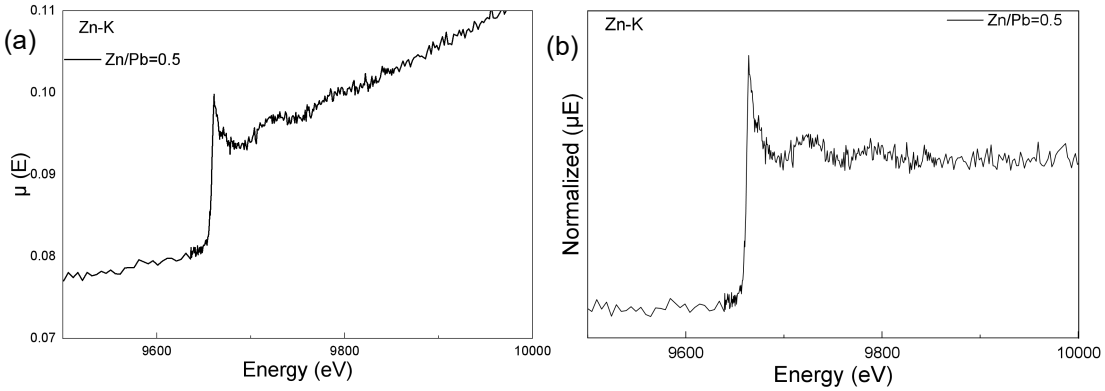

Figure S11. (a) raw Zn K-edge X-ray absorption spectra and (b) the corresponding normalized spectra for $CsPbI_3$ QDs at Zn/Pb=0.5. While the spectra confirm Zn incorporation across the doping series, the signal-to-noise ratio is insufficient for quantitative EXAFS fitting.

References

1 L. Protesescu, S. Yakunin, M. I. Bodnarchuk, F. Krieg, R. Caputo, C. H. Hendon, R. X. Yang, A. Walsh, M. V. Kovalenko, *Nano Letters*, 2015, **15**, 3692-3696.

2 Y. Zhang, T. D. Siegler, C. J. Thomas, M. K. Abney, T. Shah, A. De Gorostiza, R. M. Greene, B. A. Korgel, *Chemistry of Materials*, 2020, **32** , 5410-5423.

3 S. Sun, D. Yuan, Y. Xu, A. Wang, Z. Deng, *ACS Nano*, 2016, **10**, 3648-3657.

4 M. T. Dove, G. Li, *Nuclear Analysis*, 2022, **1**, 37-70.

5 B. Ravel, M. Newville, *Journal of Synchrotron Radiation*, 2005, **12**, 537-541.

6 H. Funke, M. Chukalina, A. C. Scheinost, *Journal of Synchrotron Radiation*, 2007, **14** , 426-432.